Article

Inorganic Cluster Syntheses of TM-Doped Quantum Dots (CdSe, CdS, CdSe/CdS): Physical Property Dependence on Dopant Locale

Paul I. Archer, Steven A. Santangelo, and Daniel R. Gamelin

J. Am. Chem. Soc., **2007**, 129 (31), 9808-9818• DOI: 10.1021/ja072436l • Publication Date (Web): 13 July 2007

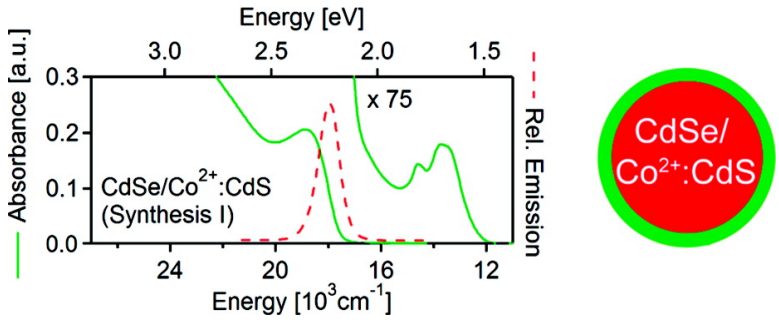

More About This Article

Additional resources and features associated with this article are available within the HTML version:

- Supporting Information
- Links to the 6 articles that cite this article, as of the time of this article download
- Access to high resolution figures
- Links to articles and content related to this article
- Copyright permission to reproduce figures and/or text from this article

View the Full Text HTML

J|A|C|S
ARTICLES
Published on Web 07/13/2007

Inorganic Cluster Syntheses of TM^{2+}-Doped Quantum Dots (CdSe, CdS, CdSe/CdS): Physical Property Dependence on Dopant Locale

Paul I. Archer, Steven A. Santangelo, and Daniel R. Gamelin*

Contribution from the Department of Chemistry, University of Washington, Seattle, Washington 98195-1700

Received April 16, 2007; E-mail: gamelin@chem.washington.edu

Abstract: A series of colloidal transition-metal-doped chalcogenide semiconductor nanocrystals (TM^{2+}:CdSe, TM^{2+}:CdS, etc.) has been prepared by thermal decomposition of inorganic cluster precursors. It is shown through extensive spectroscopic and structural characterization that the nanocrystals prepared following literature procedures for synthesis of TM^{2+}:CdSe nanocrystals actually possess an unintended CdSe/TM^{2+}:CdS core/shell morphology. The conditions required for successful formation of TM^{2+}:CdSe and TM^{2+}:CdS by cluster decomposition have been determined. Magneto-optical and photoluminescence spectroscopic results for this series of doped nanocrystals reveal major physical consequences of dopant localization within the shell and demonstrate the capacity to engineer dopant−carrier exchange interactions via core/shell doping strategies. The results presented here illustrate some of the remarkable and unexpected complexities that can arise in nanocrystal doping chemistries and emphasize the need for meticulous characterization to avoid false positives.

I. Introduction

Colloidal doped semiconductor nanocrystals (doped quantum dots) have drawn considerable attention in recent years.[1] Such materials have been shown to display unusually large magneto-optical effects,[2−7] efficient sensitized impurity luminescence,[2,8−11] and interesting quantum size effects on impurity−carrier binding energies.[12] The syntheses themselves have also provided a fertile laboratory for investigation of the basic chemistries of homogeneous nucleation and crystal growth in the presence of impurities. Dopant exclusion from critical nuclei has been suggested to be a general phenomenon,[1,4,6,13] and the modes of dopant binding to crystallite surfaces have been investigated in the context of impurity incorporation.[1,14,15]

Among the most interesting doped nanocrystal syntheses described in the literature is the so-called inorganic cluster synthesis,[16−19] in which polynuclear transition-metal (TM^{2+}) clusters such as $(Me_4N)_4[Cd_{10}Se_4(SPh)_{16}]$ and $(Me_4N)_2[Co_4(SPh)_{10}]$ undergo lyothermal degradation to yield the doped crystal lattices at the desired stoichiometries. Whereas doping of CdSe nanocrystals has proved to be relatively ineffective by standard hot-injection techniques,[15,20] this inorganic cluster method has reportedly yielded remarkably high doping levels with apparent ease. High photoluminescence quantum yields, large product yields, reasonable size distributions, and effective doping make this cluster approach the method of choice for the synthesis of doped CdSe nanocrystals.

In light of the manifold advantages of such cluster decomposition synthesis with respect to CdSe nanocrystal doping, and in light of the striking contrast between this and the more common hot-injection approach, this chemistry warrants more detailed investigation to understand precisely the origins of these differences. In this article we describe the surprising results obtained from an investigation of the inorganic cluster approach

(1) For a recent review, see: Bryan, J. D.; Gamelin, D. R. *Prog. Inorg. Chem.* **2005**, *54*, 47−126.
(2) Norris, D. J.; Yao, N.; Charnock, F. T.; Kennedy, T. A. *Nano Lett.* **2001**, *1*, 3−7.
(3) Hoffman, D. M.; Meyer, B. K.; Ekimov, A. I.; Merkulov, I. A.; Efros, A. L.; Rosen, M.; Counio, G.; Gacoin, T.; Boilot, J.-P. *Solid State Commun.* **2000**, *114*, 547−550.
(4) Schwartz, D. A.; Norberg, N. S.; Nguyen, Q. P.; Parker, J. M.; Gamelin, D. R. *J. Am. Chem. Soc.* **2003**, *125*, 13205−13218.
(5) Norberg, N. S.; Gamelin, D. R. *J. Appl. Phys.* **2005**, *99*, 08M104.
(6) Norberg, N. S.; Parks, G. L.; Salley, G. M.; Gamelin, D. R. *J. Am. Chem. Soc.* **2006**, *128*, 13195−13203.
(7) Archer, P. I.; Santangelo, S. A.; Gamelin, D. R. *Nano Lett.* **2007**, *7*, 1037−1043.
(8) Suyver, J. F.; Wuister, S. F.; Kelly, J. J.; Meijerink, A. *Phys. Chem. Chem. Phys.* **2000**, *2*, 5445−5448.
(9) Suyver, J. F.; van der Beek, T.; Wuister, S. F.; Kelly, J. J.; Meijerink, A. *Appl. Phys. Lett.* **2001**, *79*, 4222−4224.
(10) Bol, A. A.; Meijerink, A. *Phys. Rev. B* **1998**, *58*, 15997−16000.
(11) Pradhan, N.; Peng, X. *J. Am. Chem. Soc.* **2007**, *129*, 3339−3347.
(12) Norberg, N. S.; Dalpian, G. M.; Chelikowsky, J. R.; Gamelin, D. R. *Nano Lett.* **2006**, *6*, 2887−2892.
(13) Bryan, J. D.; Schwartz, D. A.; Gamelin, D. R. *J. Nanosci. Nanotechnol.* **2005**, *5*, 1472−1479.
(14) Radovanovic, P. V.; Gamelin, D. R. *J. Am. Chem. Soc.* **2001**, *123*, 12207−12214.
(15) Erwin, S. C.; Zu, L. J.; Haftel, M. I.; Efros, A. L.; Kennedy, T. A.; Norris, D. J. *Nature* **2005**, *436*, 91−94.
(16) Hanif, K. M.; Meulenberg, R. W.; Strouse, G. F. *J. Am. Chem. Soc.* **2002**, *124*, 11495−11502.
(17) Magana, D.; Perera, S. C.; Harter, A. G.; Dalal, N. S.; Strouse, G. F. *J. Am. Chem. Soc.* **2006**, *128*, 2931−2939.
(18) Meulenberg, R. W.; Van Buuren, T.; Hanif, K. M.; Willey, T. M.; Strouse, G. F.; Terminello, L. J. *Nano Lett.* **2004**, *4*, 2277−2285.
(19) Raola, O. E.; Strouse, G. F. *Nano Lett.* **2002**, *2*, 1443−1447.
(20) Mikulec, F. V.; Kuno, M.; Bennati, M.; Hall, D. A.; Griffin, R. G.; Bawendi, M. G. *J. Am. Chem. Soc.* **2000**, *122*, 2532−2540.

10.1021/ja072436l CCC: $37.00

as applied to doping CdSe nanocrystals. Following literature methods, nanocrystals were grown from the cluster precursors $(Me_4N)_4[Cd_{10}Se_4(SPh)_{16}]$ and $(Me_4N)_2[Co_4(SPh)_{10}]$. These conditions were discovered to result in thiolate decomposition, yielding unintended CdSe/CdS core/shell heterostructures. Quite unexpectedly, all of the Co^{2+} was found to segregate into the CdS nanocrystal shells. With this new information in hand, modified conditions for successful synthesis of doped CdSe nanocrystals by cluster decomposition have been identified, and the formation of doped CdSe nanocrystals under these new conditions has been demonstrated.

The experimental distinction between the target doped CdSe nanocrystals and the unintended doped CdSe/TM^{2+}:CdS core/shell nanocrystals has relied on application of sensitive dopant-specific spectroscopic techniques. Although the differences appear subtle from the perspective of dopant electronic structure, the physical properties (luminescence, magneto-optical) of the doped core/shell nanocrystals are substantially different from those of the desired doped CdSe nanocrystals. These physical differences are shown to derive from reduced dopant−exciton coupling in the core/shell nanocrystals and illustrate the capacity to engineer dopant−carrier exchange interactions via core/shell doping strategies. Finally, the chemical origins of the observed dopant segregation under literature synthetic conditions are discussed in terms of hard−soft acid−base principles.

II. Experimental Section

A. Nanocrystal Syntheses. The inorganic clusters $(Me_4N)_4[Cd_{10}Se_4(SPh)_{16}]$, $(Me_4N)_2[Cd_4(SPh)_{10}]$, $(Me_4N)_2[Cd_4(SePh)_{10}]$, and $(Me_4N)_2[Co_4(SPh)_{10}]$ were prepared following the general procedures outlined by Dance et al.,[21] where SPh^- is phenylthiolate and $SePh^-$ is phenylselenide. Briefly, the thiol-terminated inorganic cluster, $(Me_4N)_2[Cd_4(SPh)_{10}]$, was prepared at room temperature under inert (N_2) conditions by addition of $Cd(NO_3)_2{\cdot}4H_2O$ (17 mmol) in methanol (15 mL) to an equimolar solution of triethylamine and benzenethiol (45 mmol) in methanol (15 mL). A solution of tetramethylammonium chloride (19 mmol) in methanol (10 mL) was added, and the mixture was allowed to crystallize at 0 °C under N_2. The crystalline product was filtered, washed repeatedly with methanol, and dried under vacuum. $(Me_4N)_2[Co_4(SPh)_{10}]$ and $(Me_4N)_2[Cd_4(SePh)_{10}]$ were prepared by substituting $Co(NO_3)_2{\cdot}6H_2O$ and benzeneselenol for $Cd(NO_3)_2{\cdot}4H_2O$ and benzenethiol, respectively. $(Me_4N)_4[Cd_{10}Se_4(SPh)_{16}]$ was prepared by addition of equimolar amounts of $(Me_4N)_2[Cd_4(SPh)_{10}]$ and Se powder (8.9 mmol) to a solution of acetonitrile (10 mL) at room temperature, followed by stirring for 3 h. The mixture was then heated to 75 °C, and ∼135 mL of acetonitrile was added until the solid had dissolved. The solution was then allowed to crystallize at room temperature. Using these clusters as precursors, three different chalcogenide nanocrystals were synthesized according to the following approaches.

Synthesis I. In this procedure, 10.8 g of hexadecylamine (HDA, $C_{16}H_{35}N$, 90%, Acros) was degassed under vacuum at 130 °C for 1.5 h. The reaction vessel was placed under N_2 and the temperature reduced to 60 °C, at which point 0.6 g of $(Me_4N)_4[Cd_{10}Se_4(SPh)_{16}]$ and 0.2 g of $(Me_4N)_2[Co_4(SPh)_{10}]$ were introduced. Experiments were also performed using 0.009 g of $CoCl_2{\cdot}6H_2O$, degassed in HDA, in place of $(Me_4N)_2[Co_4(SPh)_{10}]$ and yielded the same results. The temperature was increased to 130 °C, maintained for 3 h, and then slowly increased to 230 °C and kept constant until the desired nanocrystal size was achieved. After growth, the solution was rapidly cooled to <100 °C, and the particles were isolated by addition of ∼5 mL of toluene and ∼30 mL of methanol. The isolated nanocrystals were then resuspended in toluene. The process of precipitation with methanol followed by resuspension in toluene was repeated three times to remove excess reagents. The nanocrystals were divided into two batches, the first capped with pyridine and the second with trioctylphosphine oxide (TOPO, 90%, Aldrich). Pyridine surface capping was conducted according to literature techniques:[17,20] the precipitated nanocrystals were suspended in pyridine and stirred at 70 °C for 12 h, at which point they were precipitated with heptane and resuspended in pyridine. This process was repeated two more times (5 h each), followed by surface exchange with HDA. TOPO capping was achieved by gently heating the precipitated nanocrystals in TOPO at 120 °C under nitrogen for ∼5 min. Special care must be taken to remove any residual methanol before heating at 120 °C. The nanocrystals were precipitated by a mixture of toluene and ethanol and resuspended in toluene.

Synthesis II. Doped CdS nanocrystals were prepared in the same manner as above, except that 0.1 g each of $(Me_4N)_2[Co_4(SPh)_{10}]$ and $(Me_4N)_2[Cd_4(SPh)_{10}]$ were added in place of the decamer. Surface-bound dopants were removed by TOPO as described above. For ease of synthesis, $CoCl_2{\cdot}6H_2O$ can be substituted for the cobalt tetramer, provided that the reaction temperature is increased to ∼250 °C.

Synthesis III. Doped CdSe nanocrystals were synthesized from $(Me_4N)_2[Cd_4(SePh)_{10}]$ as described previously for both Mn^{2+} and Co^{2+} dopants.[7] $CoCl_2{\cdot}6H_2O$ and 10.8 g of HDA were degassed under vacuum at 130 °C for 1.5 h. The reaction vessel was placed under N_2 and the temperature reduced to <80 °C, at which point 0.2 g of $(Me_4N)_2[Cd_4(SePh)_{10}]$ and 0.02 g of Se powder were introduced. The temperature was increased to 130 °C and maintained for 1.5 h. The temperature was then slowly increased to 215 °C and kept constant until the desired nanocrystal size was achieved. After growth, the solution was rapidly cooled to <100 °C, and the particles were isolated by addition of a mixture of toluene and methanol, followed by centrifugation and resuspension in toluene. The process of precipitation with methanol followed by resuspension in toluene was repeated three times to remove excess reagents. Adventitious Co^{2+} was removed by sonicating the suspended nanocrystals in the presence of TOPO, followed by precipitation, centrifugation, and resuspension in toluene.

B. Physical Characterization. Absorption spectra (300 K) of colloidal nanocrystals were collected using 1 cm cuvettes and a Cary 500 (Varian) spectrophotometer. Luminescence spectra were measured in 1 cm × 1 cm fluorescence cuvettes on a Jobin Yvon FluoroMax-2 fluorimeter. Colloidal nanocrystals were drop-coated onto quartz disks to form films for low-temperature electronic absorption and magnetic circular dichroism (MCD) measurements. Low-temperature absorption and MCD spectra were collected simultaneously using an Aviv 40DS spectropolarimeter and a high-field superconducting magneto-optical cryostat (Cryo-Industries SMC-1659 OVT) with a variable-temperature sample compartment positioned in the Faraday configuration. MCD intensities were measured as the differential absorbance, $\Delta A = A_L - A_R$, where A_L and A_R refer to the absorption of left and right circularly polarized photons following the sign convention of Piepho and Schatz[22] and are reported as $\theta(\text{mdeg}) = 32980\Delta A/A$. Powder X-ray diffraction (XRD) data were collected using a 12 kW Rigaku Rotaflex RTP300 X-ray diffractometer. X-ray photoelectron spectroscopy (XPS) data were collected using a modified SSL-300 spectrometer equipped with a monochromatic Al Kα X-ray source and a concentric hemispherical analyzer. Binding energies were calibrated using Au foils at Au ($4f_{7/2}$ = 83.943 eV) under a base pressure of ∼2×10^{-8} Torr. The shifts caused by charging effects because of the insulating substrate were corrected using a reference peak, C(1s), at 284.6 eV. Transmission electron microscopy (TEM) images were obtained using a JEOL 2010F transmission electron microscope. The Co^{2+} concentrations were determined quantitatively using an inductively coupled plasma atomic

(21) Dance, I. G.; Choy, A.; Scudder, M. L. *J. Am. Chem. Soc.* **1984**, *106*, 6285−6295.

(22) Piepho, S. B.; Schatz, P. N. *Group Theory in Spectroscopy with Applications to Magnetic Circular Dichroism*; Wiley: New York, 1983.

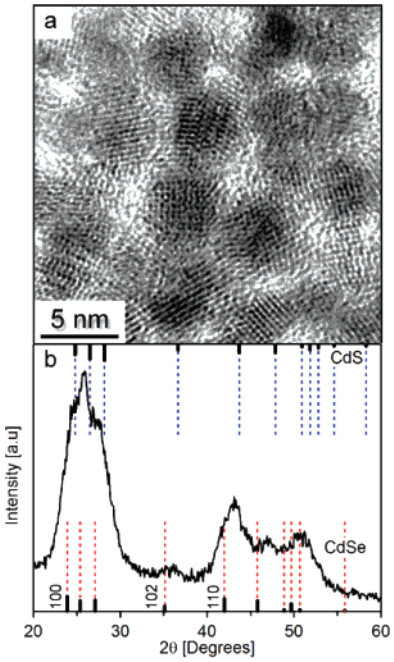

Figure 1. (a) TEM image of $d \approx 3.7$ nm nanocrystals doped with 2.0% Co^{2+} and (b) X-ray diffraction data of $d \approx 3.4$ nm 0.91% Co^{2+} nanocrystals. The black posts correspond to wurtzite CdSe (bottom) and wurtzite CdS (top).

emission spectrometer (ICP-AES, Jarrel Ash model 955) after acid digestion of the samples.

III. Results and Analysis

A. Unintentional Formation of CdSe/CdS Nanocrystal Heterostructures by Synthesis I. 1. Results from Synthesis I. The first group of chalcogenide nanocrystals were synthesized according to literature procedures (Synthesis I) reported to produce CdSe and TM^{2+}:CdSe nanocrystals.[16,17,19,23] Essentially identical results were obtained using either $(Me_4N)_2[Co_4(SPh)_{10}]$ or $CoCl_2 \cdot 6H_2O$ as the dopant source. Figure 1 shows representative TEM and powder XRD data for two batches of Co^{2+}-doped nanocrystals. The posts in Figure 1b correspond to bulk wurtzite CdSe (bottom) and CdS (top) peak positions and relative powder diffraction intensities. The nanocrystals appear spherical in shape and have a wurtzite crystal structure. A Scherrer[24] analysis of the 110 peak in Figure 1b yielded an average nanocrystal diameter of $d \approx 3.4$ nm. As anticipated from Vegard's law for the substitution of Co^{2+} for Cd^{2+} in the wurtzite lattice, the nanocrystals exhibited XRD peak shifts relative to wurtzite CdSe that indicate lattice contraction. Analysis of the XRD angles using the relationship between Co^{2+} doping and lattice parameter reported previously[16] for the same synthetic procedure would suggest ~17% Co^{2+} substitution into the CdSe nanocrystals (i.e., $Cd_{0.83}Co_{0.17}Se$). This result is in stark contrast with the concentration of only 0.91% Co^{2+} determined analytically for the same batch of nanocrystals.

Ligand-field electronic absorption spectroscopy was used to monitor the speciation of the Co^{2+} ions throughout the course of the synthesis and processing. This technique has previously been shown to allow differentiation between substitutional and surface-bound Co^{2+} ions in Co^{2+}:CdS[14] and Co^{2+}:ZnO nanocrystals[4,25] and to provide a probe of alloy composition in Co^{2+}-doped $Cd_{1-x}Zn_xSe$ nanocrystals.[26] Electronic absorption spectra obtained at 300 K in the Co^{2+} $^4A_2(F) \rightarrow {}^4T_1(P)$ ligand-field energy region at various stages of the preparative procedure are presented in Figure 2. The as-prepared nanocrystals show a broad, intense feature indicative of multiple Co^{2+} species in multiple low-symmetry coordination environments (i.e., on nanocrystal surfaces, in solution, internally doped, etc.). In an effort to remove the adventitious Co^{2+}, the as-prepared nanocrystals were split into two batches: one for TOPO surface exchange and the other for pyridine surface exchange (see Experimental Section). As can be seen in Figure 2, the pyridine-exchanged nanocrystals show absorption features very similar to those of the as-prepared nanocrystals, revealing that multiple Co^{2+} species still remain. In contrast, the TOPO-capped nanocrystals show a narrower ligand-field band shape reflecting a more uniform Co^{2+} speciation. After TOPO capping, the Co^{2+} $^4A_2(F) \rightarrow {}^4T_1(P)$ absorption band shape closely resembles those of other substitutional Co^{2+} ions in II−VI lattices.[4,6,7,14] These data demonstrate the ability of this TOPO-capping procedure to remove surface-bound transition metal ions, leaving behind only those incorporated within the internal volumes of the nanocrystals. These data also demonstrate the inability of the popular pyridine exchange process to eliminate adventitious TM^{2+} ions with sufficient reliability. From the intensities in Figure 2, it is estimated that over ~60% of the Co^{2+} in the pyridine-exchanged nanocrystals was not actually doped within the nanocrystals. The presence of adventitious TM^{2+} ions will result in false positive claims of doping and in misinterpretation of physical properties, so great care must be taken to demonstrate the efficacy of any cleaning method used.

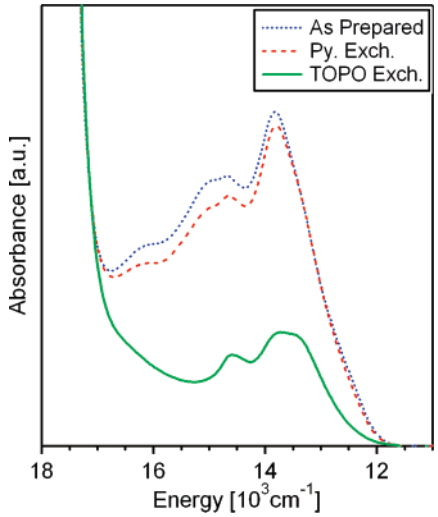

Figure 2. 300 K electronic absorption spectra in the Co^{2+} $^4A_2(F) \rightarrow {}^4T_2(P)$ ligand-field region after various ligand-exchange procedures are applied to remove adventitious Co^{2+}. The as-prepared (···) and pyridine-exchanged (- - -) particles show very similar broad absorption bands, indicative of multiple cobalt species. The TOPO-exchanged particles (—) show only the narrower absorption feature of substitutionally doped Co^{2+} (see text).

2. Discrepancies between Anticipated and Observed Products of Synthesis I. 2.1. Sizes Estimated from Electronic

(23) Cumberland, S. L.; Hanif, K. M.; Javier, A.; Khitrov, G. A.; Strouse, G. F.; Woessner, S. M.; Yun, C. S. *Chem. Mater.* **2002**, *14*, 1576−1584.
(24) West, A. R. *Solid State Chemistry*; Wiley: Chichester, 1992.
(25) Radovanovic, P. V.; Norberg, N. S.; McNally, K. E.; Gamelin, D. R. *J. Am. Chem. Soc.* **2002**, *124*, 15192−15193.
(26) Santangelo, S. A.; Hinds, E. A.; Vlaskin, V. A.; Archer, P. I.; Gamelin, D. R. *J. Am. Chem. Soc.* **2007**, *129*, 3973−3978.

Absorption, TEM, and XRD. Recent reports[27] have established a relationship between the wavelength of the first excitonic absorption maximum in CdSe nanocrystals and the nanocrystal size, as determined by XRD or TEM. As demonstrated previously,[7] this relationship is also valid for doped CdSe nanocrystals at the impurity concentrations under consideration here. When these analyses are applied to the nanocrystals prepared by Synthesis I, however, the sizes calculated from absorption spectroscopy are consistently smaller than those determined by TEM and XRD. For example, the average diameter of the 2.0% Co^{2+}-doped nanocrystals of Figure 1a determined from their excitonic absorption spectrum (2.69 nm) is significantly smaller than those determined by XRD (3.8 nm) and TEM (3.7 nm). A similar discrepancy is found for the 0.91% Co^{2+}-doped nanocrystals of Figures 1b and 3 (2.56 nm from absorption vs 3.4 nm from XRD).[28] Clearly, the experimental products obtained from Synthesis I differ from the anticipated products.

2.2. Ligand-Field Transition Energies and Excitonic Luminescence. The 300 K electronic absorption and photoluminescence spectra of TOPO-capped (surface-cleaned) 0.91% Co^{2+}-doped nanocrystals are shown in Figure 3. The excitonic absorption and luminescence features of CdSe at ~19 000 cm^{-1} agree well with those reported previously for Co^{2+}:CdSe nanocrystals, which were reported to have excitonic luminescence quantum yields as large as $\phi_{Lum}^{ex} \approx 0.19$.[16] As described above, however, the $^4A_2(F) \rightarrow {}^4T_1(P)$ ligand-field transition of tetrahedral Co^{2+} is also observed at ~13 800 cm^{-1}, below the nanocrystal band edge absorption. Co^{2+} doping should therefore quench the CdSe quantum dot excitonic luminescence (Scheme 1).

From eq 1, the excitonic luminescence quantum yield (ϕ_{Lum}^{ex}) is determined by the ratio of the excitonic radiative rate constant (k_r^{ex}) to the sum of all excitonic decay rate constants (where k_{nr}^i indicates the *i*th nonradiative pathway). In Co^{2+}-doped CdSe

$$\phi_{Lum}^{ex} = \frac{k_r^{ex}}{k_r^{ex} + \sum_i k_{nr}^i} \qquad (1)$$

nanocrystals, nonradiative energy transfer to Co^{2+} ($k_{nr}^{Co^{2+}}$ in Scheme 1) should dominate all other relaxation kinetics and consequently lead to excitonic emission quantum yields close to zero. Indeed, Co^{2+} is generally an efficient exciton luminescence trap in II−VI semiconductors because of its multiple sub-band-gap ligand-field energy levels. The concomitant observation of CdSe excitonic luminescence and sub-band-gap Co^{2+} ligand-field absorption in the nanocrystals prepared by Synthesis I thus raises serious doubts about successful Co^{2+} incorporation into these CdSe nanocrystals.

Upon closer comparison to literature,[29,30] the Co^{2+} ligand-field absorption spectrum is found to be inconsistent with Co^{2+} doping of CdSe. Instead, it quite unexpectedly resembles the

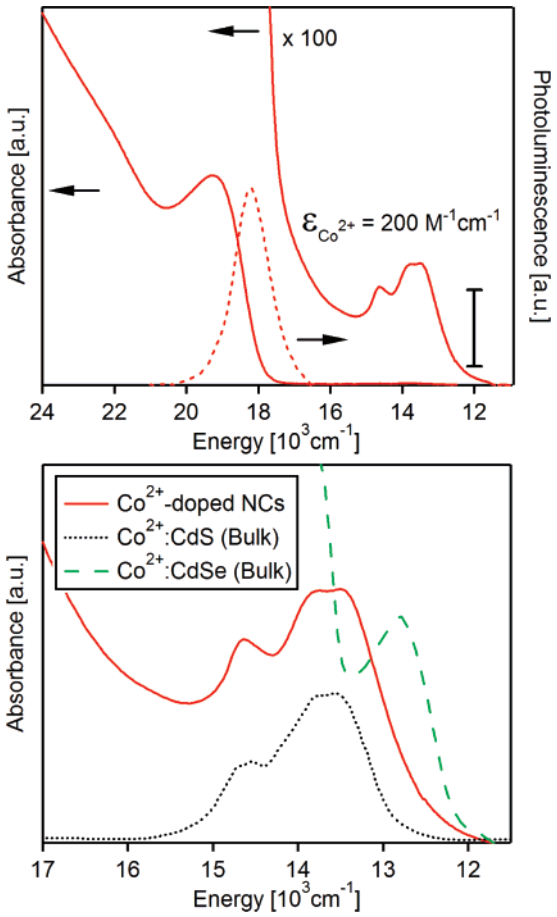

Figure 3. (Top) 300 K electronic absorption (solid) and photoluminescence (dashed) spectra of TOPO-capped $d \approx 3.4$ nm 0.91% Co^{2+}-doped nanocrystals prepared by Synthesis I, suspended in toluene. (Bottom) 300 K electronic absorption spectra in the Co^{2+} $^4A_2(F) \rightarrow {}^4T_1(P)$ ligand-field region. Co^{2+} in the nanocrystals prepared by Synthesis I closely resembles Co^{2+} in CdS but not Co^{2+} in CdSe. Bulk absorption spectra adapted from refs 29 and 30.

Scheme 1

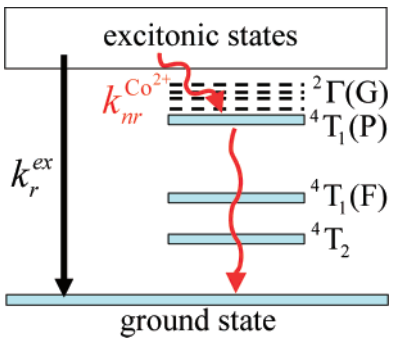

spectrum of Co^{2+} in CdS,[14,29,31] which has its $^4A_2(F) \rightarrow {}^4T_1(P)$ transition shifted to higher energy by ~1000 cm^{-1} relative to that of Co^{2+} in CdSe (Figure 3). This inconsistency between anticipated and observed $^4T_1(P)$ energies, combined with the observation of CdSe luminescence despite the trapping properties of Co^{2+}, suggests that Synthesis I does not actually yield Co^{2+}-doped CdSe nanocrystals as expected. These data instead suggest that Synthesis I forms both CdSe and Co^{2+}-doped CdS as segregated crystalline phases.

(27) Yu, W. W.; Qu, L.; Guo, W.; Peng, X. *Chem. Mater.* **2003**, *15*, 2854−2860.
(28) Re-examination of the CdSe nanocrystal data in ref 23 shows that the sizes calculated from their electronic absorption spectroscopy are also consistently ~0.9 nm smaller than those estimated from their TEM images.
(29) Weakliem, H. A. *J. Chem. Phys.* **1962**, *36*, 2117−2140.
(30) Langer, J. M.; Baranowski, J. M. *Phys. Stat. Sol. (b)* **1971**, *44*, 155−166.
(31) Pappalardo, R.; Dietz, R. E. *Phys. Rev.* **1961**, *123*, 1188−1203.

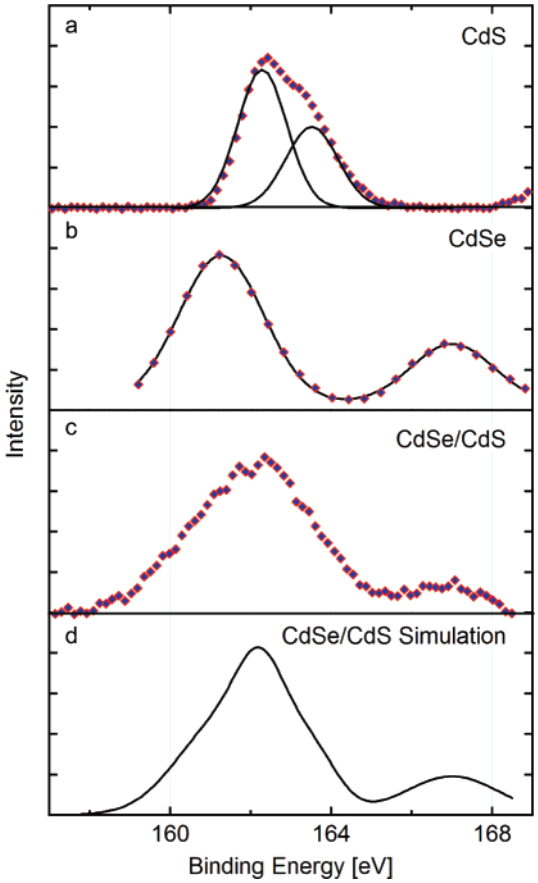

Figure 4. XPS spectra of (a) 1.5% Co^{2+}:CdS from Synthesis II, (b) undoped CdSe nanocrystals (adapted from ref 33), and (c) 0.91% Co^{2+}-doped nanocrystals from Synthesis I. The solid lines represent best fits using two Gaussians. The spectrum in (d) is a linear combination of the spectra from (a) and (b), simulating a mixture of CdSe and CdS. The fractional S^{2-} composition estimated from this analysis is $S^{2-}/(S^{2-} + Se^{2-}) = 0.62$.

It should be noted that, whereas Co^{2+}:CdSe and Co^{2+}:CdS are readily differentiated using electronic absorption spectroscopy, Mn^{2+}:CdSe and Mn^{2+}:CdS are not easily differentiated by electron paramagnetic resonance (EPR) spectroscopy because the Mn^{2+} EPR parameters in these two lattices are very similar to one another (in wurtzite CdS, $g = 2.002$ and $A = -66.0 \times 10^{-4}$ cm^{-1}; in wurtzite CdSe, $g = 2.004$ and $A = -62.2 \times 10^{-4}$ cm^{-1}).[32] Extreme care must therefore be taken when concluding successful doping on the basis of EPR spectroscopy alone.[5]

2.3. X-ray Photoelectron Spectroscopy. Conclusive evidence for CdS formation by Synthesis I is obtained using XPS, which allows the relative chalcogenide anion compositions of the nanocrystals to be determined. Figure 4 shows XPS spectra of (a) 1.5% Co^{2+}:CdS nanocrystals (from Synthesis II, *vide infra*), (b) an undoped CdSe reference sample (adapted from ref 33), and (c) 0.91% Co^{2+}-doped nanocrystals from Synthesis I, and Gaussian fits of the CdS and CdSe data (solid lines in panels a and b). The XPS spectrum of the nanocrystals from Synthesis I (Figure 4c) clearly possesses contributions from both CdS and CdSe. The data were therefore simulated (Figure 4d) using a linear combination of the CdS and CdSe intensities from Figure 4a,b. From this analysis, the fractional sulfide composition in the nanocrystals prepared by Synthesis I is estimated to be $S^{2-}/(S^{2-} + Se^{2-}) = 0.62$. These XPS spectra corroborate the conclusion drawn from electronic absorption spectroscopy (Figure 3) that Synthesis I yields both CdSe and Co^{2+}:CdS as products.

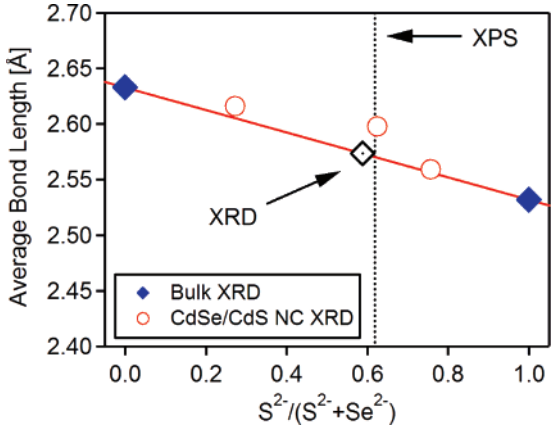

Figure 5. Average cation−anion bond lengths as a function of fractional sulfide composition: (◆) bulk wurtzite CdSe and CdS; (○) CdSe/CdS core/shell nanocrystals (adapted from ref 33); (◇) average cation−anion bond length from the XRD data in Figure 1b. The fractional sulfide composition from the XRD data is $S^{2-}/(S^{2-} + Se^{2-}) = 0.59$. The result determined by XPS in Figure 4 ($S^{2-}/(S^{2-} + Se^{2-}) = 0.62$) is plotted for comparison (- - -).

2.4. X-ray Diffraction. Finally, CdS formation by Synthesis I is also evident from the XRD data. As described above, the XRD shifts in Figure 1 are too large to be caused by the relatively small concentration of Co^{2+} present in these nanocrystals. Instead, this line shift reflects the co-formation of CdSe and CdS lattices during synthesis. In a II−VI $AE_{1-x}Y_x$ random alloy nanocrystal (e.g., $CdSe_{1-x}S_x$), the XRD peak positions and average bond lengths will follow Vegard's law,[26,34] showing an approximately linear variation with x between the AE and AY endpoints. Figure 5 plots the anticipated relationship between the fractional S^{2-} anion composition and the average cation−anion bond length calculated from the 110 diffraction peak for the CdSe and CdS pair of lattices. Interestingly, CdSe/CdS core/shell nanocrystal XRD data from ref 33 also follow this behavior, falling very nearly on the same Vegard's law line. This comparison indicates that, to a good approximation, the same plot describes core/shell nanocrystals and random alloys. Using this plot, the XRD angles from Figure 1b ($d \approx 3.4$ nm) can be analyzed to estimate the fractional S^{2-} content of the nanocrystals prepared by Synthesis I. From this analysis, $S^{2-}/(S^{2-} + Se^{2-}) = 0.59$ is determined (Figure 5). This value agrees remarkably well with that determined from XPS ($S^{2-}/(S^{2-} + Se^{2-}) = 0.62$), providing strong support for the conclusion that the product prepared by Synthesis I contains a substantial amount of CdS.

2.5. Summary of Synthesis I. The large XRD shift (Figures 1b and 5), the unquenched excitonic emission (Figure 3), and the shifted Co^{2+} ligand-field transition (Figure 3) all provide evidence against simple substitutional Co^{2+} incorporation into CdSe nanocrystals by Synthesis I. The Co^{2+} ligand-field electronic absorption and XPS spectra (Figures 3 and 4) suggest that this synthesis instead forms CdS in addition to CdSe.

(32) Title, R. S. *Phys. Rev.* **1963**, *131*, 2503−2504.
(33) Peng, X.; Schlamp, M. C.; Kadavanich, A. V.; Alivisatos, A. P. *J. Am. Chem. Soc.* **1997**, *119*, 7019−7029.
(34) Furdyna, J. K., Kossut, J., Eds. *Diluted Magnetic Semiconductors*; Semiconductors and Semimetals 25; Willardson, R. K., Beer, A. C., Series Eds.; Academic Press: New York, 1988.

Quantitative analysis of XPS and XRD data indicates an anion stoichiometry of $S^{2-}/(S^{2-} + Se^{2-}) = 0.62$ for the $d \approx 3.4$ nm nanocrystals shown in Figure 3.

Three limiting scenarios can be identified and tested against this collection of experimental data: (i) formation of two distinct groups of nanocrystals (CdSe and Co^{2+}:CdS), (ii) formation of Co^{2+}-doped random alloy $CdSe_{1-x}S_x$ nanocrystals, and (iii) formation of CdSe/Co^{2+}:CdS core/shell structures. As illustrated by Figure 3, the ligand-field absorption spectra show that the Co^{2+} ions are uniformly coordinated by four S^{2-} ligands in an environment indistinguishable from CdS. Specifically, the Co^{2+} ligand-field electronic absorption spectra are inconsistent with Co^{2+}-doped $CdSe_{1-x}S_x$ nanocrystals, which would show $^4T_1$-(P) transition energies between those of Co^{2+}:CdSe and Co^{2+}:CdS.[26] This rules out scenario ii. As will be discussed in section D, the MCD spectra of these nanocrystals are inconsistent with separate CdSe and Co^{2+}:CdS nanocrystals (scenario i) and instead implicate formation of CdSe/Co^{2+}:CdS heterostructures (scenario iii). The experimental XPS spectrum of the nanocrystals formed by Synthesis I (Figure 4c) is very similar to that reported[35] previously for CdSe/CdS core/shell nanocrystals and is thus consistent with scenario iii. Using the experimental anion fraction of $S^{2-}/(S^{2-} + Se^{2-}) = 0.62$, the diameter of the nanocrystals determined from XRD ($d \approx 3.4$ nm), and approximating the particles as spherical (Figure 1), a CdS shell thickness of 0.45 nm (i.e., CdSe core $d \approx 2.5$ nm, CdSe/CdS core/shell $d \approx 3.4$ nm) can be estimated from the XPS spectra. This corresponds to an average CdS shell thickness of 1−2 monolayers, although anisotropic shell growth is likely.[36] The difference (∼0.9 nm) between these core and core/shell diameters is remarkably similar to that obtained from electronic absorption spectroscopy and described in section 2.1 (∼0.9 nm). Collectively, these data all suggest that Synthesis I leads to formation of CdSe/CdS core/shell nanocrystals and that Co^{2+} dopants segregate quantitatively into the CdS layers. Figure 6a summarizes the 300 K electronic absorption and luminescence spectra of TOPO-capped 2.0% Co^{2+}-doped nanocrystals prepared by Synthesis I, for comparison with those prepared by Syntheses II and III as discussed below.

B. Synthesis of Doped CdS Nanocrystals by Thiolate Decomposition. Since the phenylthiolate (SPh^-) associated with the cluster precursors $(Me_4N)_4[Cd_{10}Se_4(SPh)_{16}]$ and $(Me_4N)_2[Co_4(SPh)_{10}]$ is the only potential source of sulfur in Synthesis I, we hypothesized that the experimental conditions of Synthesis I must lead to decomposition of SPh^- to liberate S^{2-}, which subsequently reacts with Cd^{2+} to form CdS. To test this hypothesis, a trial reaction was performed that excluded all sources of selenium but included Co^{2+} and Cd^{2+} and had SPh^- as the only potential source of S^{2-} (Synthesis II, see Experimental Section). This reaction does indeed yield high-quality spherical nanocrystals having XRD peak positions consistent with CdS (see Supporting Information). Figure 6b shows the 300 K electronic absorption and luminescence spectra of one such sample prepared by Synthesis II, having a cobalt cation mole fraction of 1.5%, as determined by ICP-AES. Both the excitonic (∼23 000 cm^{-1}) and Co^{2+} ligand-field (∼13 800 cm^{-1}) transitions are observed in the absorption spectrum of the nanocrystals made by Synthesis II (Figure 6b). The $^4A_2$-(F) → $^4T_1$(P) transition energy is the same as those of bulk Co^{2+}:CdS (see Supporting Information, Figure S2),[29] nanocrystalline Co^{2+}:CdS prepared by inverted micelle synthesis,[14] and most importantly, the nanocrystals prepared by Synthesis I (Figure 6a). These data provide strong evidence in support of the hypothesis that CdS formation derives from the decomposition of SPh^- under these experimental conditions. The formation of II−VI nanocrystals via thermal degradation of thiolate-bound inorganic clusters has precedent.[37] A similar sulfide shell growth may also explain the enhanced luminescence quantum yields and shifted luminescence energies observed when Mn^{2+}:ZnSe nanocrystals were heated with thiolates at 220 °C.[11]

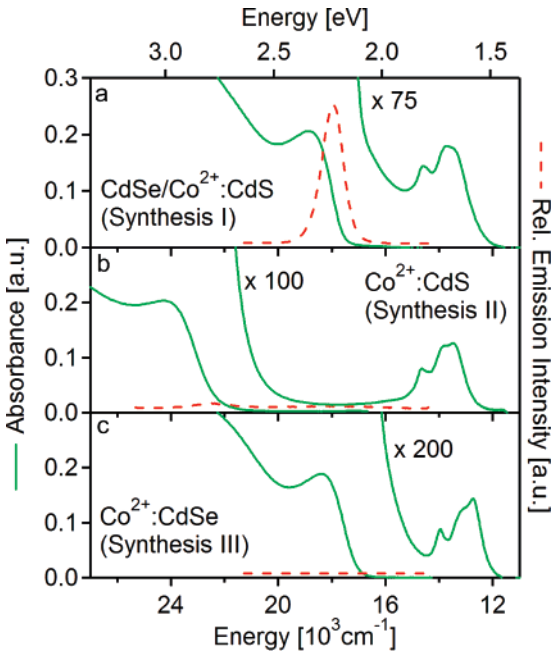

Figure 6. 300 K electronic absorption and photoluminescence spectra of TOPO-capped (a) $d \approx 3.7$ nm 2.0% Co^{2+}-doped CdSe/CdS nanocrystals, (b) $d \approx 3.8$ nm 2.2% Co^{2+}:CdS nanocrystals, and (c) $d \approx 2.9$ nm 0.85% Co^{2+}:CdSe nanocrystals, each suspended in toluene.

C. Successful Method for Synthesis of Doped CdSe Nanocrystals. Upon establishing that Synthesis I yields CdS in addition to CdSe, attempts were made to synthesize pure CdSe without using any sulfur-containing ligands. This synthesis thus involves substitution of phenylselenide for phenylthiolate in the precursor inorganic cluster. Spectroscopic results for Mn^{2+}:CdSe and Co^{2+}:CdSe nanocrystals prepared by this approach have been communicated recently.[7] Prior to this recent study,[7] neither $(Me_4N)_2[Cd_4(SePh)_{10}]$ nor related selenol-containing clusters had been used to prepare doped CdSe nanocrystals, although related clusters have been reported to yield undoped CdSe nanocrystals when heated under similar conditions.[37] A very interesting series of ternary $Zn_xCd_{1-x}E$ (E = Se, Te) nanoparticles has also been made by thermal decomposition of related clusters.[38] Figure 6c summarizes the 300 K electronic absorption and luminescence spectra of TOPO-capped 0.85% Co^{2+}:CdSe nanocrystals prepared by Synthesis III. No attempts were made to optimize the synthesis to yield narrower size distributions, which would sharpen the excitonic absorption features. The first excitonic

(35) Li, J. J.; Wang, A. Y.; Guo, W.; Keay, J. C.; Mishima, T. D.; Johnson, M. B.; Peng, X. *J. Am. Chem. Soc.* **2003**, *125*, 12567−12575.
(36) Yu, Z. G.; Guo, L.; Du, H.; Krauss, T.; Silcox, J. *Nano Lett.* **2005**, *5*, 565−570.
(37) Eichhöfer, A. *Eur. J. Inorg. Chem.* **2005**, 1245−1253.
(38) DeGroot, M. W.; Rösner, H.; Corrigan, J. F. *Chem. Eur. J.* **2006**, *12*, 1547−1554.

absorption band in Figure 6c is broader than those of the best colloidal CdSe nanocrystals prepared by hot-injection techniques, leaving room for improvement. This poorer size distribution presumably arises from concomitant nucleation and growth during lyothermal cluster decomposition, in contrast with the well-separated nucleation and growth achieved by hot-injection methods.

Initial efforts to synthesize TM^{2+}:CdSe nanocrystals by adapting Synthesis II directly using $(Me_4N)_2[Cd_4(SePh)_{10}]$ in place of $(Me_4N)_2[Cd_4(SPh)_{10}]$ yielded only undoped CdSe nanocrystals instead of doped CdSe nanocrystals (data not shown). CdSe nanocrystal doping was successful only upon addition of excess Se^0 powder (see Experimental Section, Synthesis III).[7] Although it is not yet clear precisely why excess Se^0 powder assists Co^{2+} doping of CdSe nanocrystals, it is likely that the selenium enables the formation of larger inorganic clusters, as described by eqs 2 and 3.

$$5[Cd_4(SePh)_{10}]^{2-} + 8Se^0 \rightarrow 2[Cd_{10}Se_4(SePh)_{16}]^{4-} + 8PhSeSePh + 2SePh^- \quad (2)$$

$$2[Cd_4(SePh)_{10}]^{2-} + Se^0 \rightarrow [Cd_8Se(SePh)_{16}]^{4-} + PhSeSePh + 2SePh^- \quad (3)$$

The chemistry of eq 2 is analogous to that reported[21] for synthesis of $[Cd_{10}Se_4(SPh)_{16}]^{4-}$, with the substitution of phenylselenide for the phenylthiolate ligand. The reaction in eq 3 is based on the presumption of similar reactivities for the phenylselenide and phenylthiolate clusters. Both of these reactions involve net reduction of Se^0 to Se^{2-} in the formation of higher-nuclearity clusters from Cd tetramers and can be viewed as steps along the CdSe nucleation reaction coordinate.

D. Physical Consequences of CdSe/Co^{2+}:CdS Core/Shell Structure from Synthesis I. The results in Figures 1-6 demonstrate that both CdSe and Co^{2+}:CdS are formed in Synthesis I. MCD spectroscopy provides additional valuable insight into the structural relationship between the two lattices. As described previously, MCD spectroscopy offers a powerful probe of dopant−carrier exchange interactions (sp−d exchange) in TM^{2+}-doped semiconductor nanocrystals.[2−7] The two signature features of doped quantum dots (Co^{2+}- or Mn^{2+}-doped) in MCD spectroscopy are[7] (i) inverted polarities at the band edge relative to undoped nanocrystals and (ii) TM^{2+} saturation-magnetization of the excitonic MCD intensities. Here we describe the relationship between the dopant locales, the excitonic wave functions, the existence of excitonic luminescence, and the excitonic MCD intensities of the samples prepared by Syntheses I−III.

1. Giant Excitonic Zeeman Splittings. Figure 7 compares the helium-temperature 5 T MCD spectra of 0.91% CdSe/Co^{2+}:CdS nanocrystals (Synthesis I), 1.5% Co^{2+}:CdS nanocrystals (Synthesis II), and 1.5% Co^{2+}:CdSe nanocrystals (Synthesis III). The MCD spectra of the Co^{2+}:CdS and Co^{2+}:CdSe nanocrystals both show intense negative derivative $\mathscr{A}$-term MCD features near the host band edges.[7] In both cases, these excitonic MCD features are more intense than the Co^{2+} $^4A_2(F) \rightarrow {}^4T_1(P)$ ligand-field MCD features. In Co^{2+}:CdSe, the excitonic and ligand-field transitions are both lower in energy than in Co^{2+}:CdS because of the larger cation−anion bond lengths and the smaller anion electronegativities of CdSe.

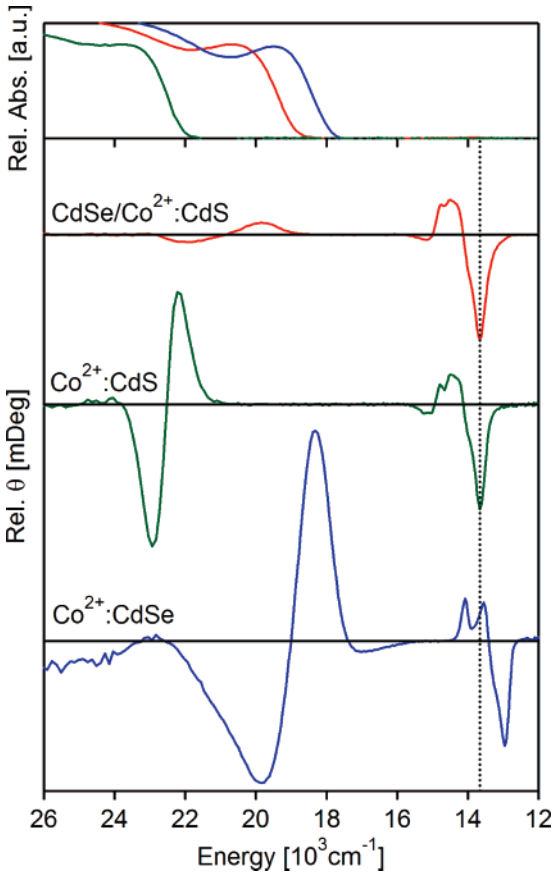

Figure 7. Low-temperature electronic absorption and 5 T MCD spectra of frozen solutions of $d \approx 3.4$ nm 0.91% CdSe/Co^{2+}:CdS nanocrystals (Synthesis I, 5 K spectra), $d \approx 4.6$ nm 1.5% Co^{2+}:CdS nanocrystals (Synthesis II, 6 K spectra), and $d \approx 2.8$ nm 1.5% Co^{2+}:CdSe nanocrystals (Synthesis III, 6 K spectra). The dotted line is a guide for the eye.

Figure 8 shows the helium-temperature MCD saturation-magnetization probed in the $^4A_2(F) \rightarrow {}^4T_1(P)$ ligand-field region and at the first excitonic transition of the semiconductor host. The solid lines show the $S = {}^3/_2$ spin-only saturation-magnetization calculated from the Brillouin function (eq 4)

$$M = -N_0 x_{eff} g\mu_B \langle S_z \rangle = \frac{1}{2} N_0 x_{eff} g\mu_B \left[(2S+1) \coth\left((2S+1)\left(\frac{g\mu_B \mathbf{H}}{2kT}\right)\right) - \coth\left(\frac{g\mu_B \mathbf{H}}{2kT}\right)\right] \quad (4)$$

using the appropriate bulk parameters ($g = 2.26$, $S = {}^3/_2$ for Co^{2+}:CdS and CdSe/Co^{2+}:CdS; $g = 2.3$, $S = {}^3/_2$ for Co^{2+}:CdSe),[39] where M is the magnetization, N_0 is the number of unit cells per unit volume, x_{eff} is the effective cation mole fraction of paramagnetic ions (reduced by statistical antiferromagnetic dimer interactions[34]), μ_B is the Bohr magneton, T is the temperature, $\mathbf{H}$ is the magnetic field, $\langle S_z \rangle$ is the spin expectation value of the magnetic ions in the direction of the applied magnetic field, and k is Boltzmann's constant. All transitions show $S = {}^3/_2$ saturation-magnetization, indicating that all MCD intensity ultimately derives from the magnetization of the Co^{2+} dopants.

(39) Gennser, U.; Liu, X. C.; Vu, T. Q.; Heiman, D.; Fries, T.; Shapira, Y.; Demianiuk, M.; Twardowski, A. *Phys. Rev. B* **1995**, *51*, 9606−9611.

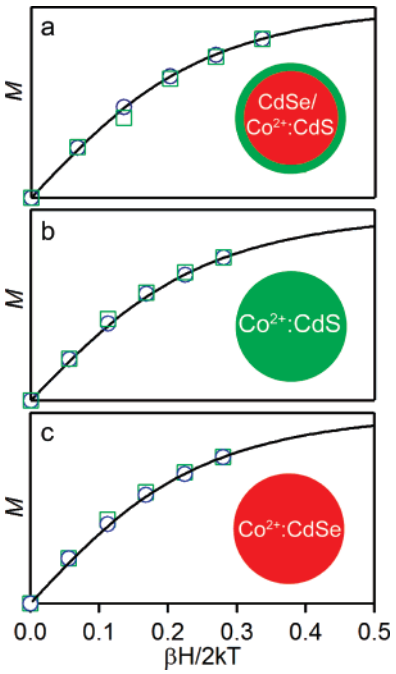

Figure 8. MCD saturation-magnetization data probed at the Co^{2+} $^4T_1(P)$ (○) and semiconductor excitonic (□) transition energies: (a) 0.91% CdSe/Co^{2+}:CdS nanocrystals of Synthesis I, 5 K data; (b) 1.5% Co^{2+}:CdS nanocrystals of Synthesis II, 6 K data; and (c) 1.5% Co^{2+}:CdSe nanocrystals of Synthesis III, 6 K data. The solid lines show the $S = {}^3/_2$ spin-only saturation-magnetization predicted by the Brillouin function (eq 4).

Several important observations can be made about the MCD spectra of the 0.91% CdSe/Co^{2+}:CdS nanocrystals prepared by Synthesis I when compared to those of the Co^{2+}:CdS and Co^{2+}:CdSe nanocrystals (Figure 7). The ligand-field MCD transition is identical to that of Co^{2+}:CdS and is clearly distinguishable from that of Co^{2+}:CdSe, indicating that the CdSe lattice is not doped. This observation confirms the conclusion drawn from the electronic absorption spectra (Figure 3) that Co^{2+} preferentially segregates into the CdS lattice. Although not doped, the CdSe band edge still shows a negative derivative $\mathscr{A}$-term MCD signal that saturates with $S = {}^3/_2$ magnetization (Figure 8a, □), indicating exchange coupling between Co^{2+} and the CdSe exciton. An upper limit of $<0.02\%$ Co^{2+} in the CdSe lattice can be estimated from quantitative analysis of the ligand-field MCD intensities. From comparison with the data for Co^{2+}:CdSe nanocrystals (Figure 7), such a small doping level could only account for an upper limit of $<\sim$10% of the observed CdSe excitonic MCD intensity for the nanocrystals from Synthesis I. The experimental excitonic MCD intensity therefore cannot be attributable to a small Co^{2+} content in the CdSe lattice but must instead derive from exchange coupling between the Co^{2+} in the CdS lattice and the exciton in the CdSe lattice. These data thus provide conclusive evidence of a hetero-interface between the Co^{2+}:CdS and CdSe lattices in these nanocrystals and, when considered along with the other experimental results, are most consistent with a CdSe/Co^{2+}:CdS core/shell heterostructure. The weak CdSe excitonic MCD intensity relative to the ligand-field MCD intensity clearly indicates a much weaker Co^{2+}−exciton exchange interaction in the core/shell nanocrystals than in either the Co^{2+}:CdS or Co^{2+}:CdSe nanocrystals (Figure 7).

Because the excitonic MCD intensities of these doped nanocrystals derive from exchange-enhanced excitonic Zeeman splittings,[7] the experimental excitonic Zeeman splitting energies can be determined by analysis of the MCD intensities. Equation 5 relates the experimental data to the Zeeman splittings.[3,6,7] Here,

$$\Delta E_{\text{Zeeman}} = -\frac{2\sigma\Delta A}{A} \tag{5}$$

σ refers to the Gaussian bandwidth of the excitonic absorption signal and $\Delta A/A$ is the maximum excitonic MCD intensity at the leading edge feature divided by the absorbance at the same energy. Application of eq 5 to the data in Figure 7 yields $\Delta E^{\text{sat.}}_{\text{Zeeman}} = -0.5 \pm 0.2$ meV for the CdSe/Co^{2+}:CdS nanocrystals from Synthesis I. This splitting is very small compared with the value of $\Delta E^{\text{sat.}}_{\text{Zeeman}} = -13.3$ meV estimated for the 1.5% Co^{2+}:CdSe nanocrystals obtained from Synthesis III[7] and the value of $\Delta E^{\text{sat.}}_{\text{Zeeman}} = -13.4$ meV estimated for the 1.5% Co^{2+}:CdS nanocrystals from Synthesis II. Importantly, the sign of the MCD intensity for the samples from Synthesis I (Figure 7) indicates that the hole−Co^{2+} (p−d) exchange energies dominate over both the electron−Co^{2+} (s−d) exchange energies and the intrinsic excitonic splittings because only the p−d exchange term flips the sign of the excitonic $\mathscr{A}$-term MCD signal.[7] These various contributions to the overall excitonic Zeeman splitting thus compete to determine the sign of the excitonic MCD feature observed experimentally.

2. Dopant−Exciton Coupling in Core/Shell Nanostructures. To illustrate the origin of the small excitonic MCD intensity in the CdSe/Co^{2+}:CdS nanocrystals of Figure 7, the electron and hole wave functions have been analyzed within the effective mass approximation.[40] Calculations were performed on idealized spherical core/shell nanostructures with infinite barriers at their surfaces. Since the true CdSe/CdS band potential offsets for these nanocrystals are not known, the natural offsets of +0.18 eV (conduction band) and −0.39 eV (valence band) were assumed, derived from *ab initio* calculations[41] based on density functional theory using pseudopotentials within the local density approximation (LDA). These offsets are similar to those calculated using the all-electron linearized augmented plane wave (LAPW) method (+0.32 eV (conduction band) and −0.42 eV (valence band))[42] and to those estimated from the differences between bulk electron affinities and ionization potentials (+0.27 eV (conduction band) and −0.51 eV (valence band)).[33,43] Similarly, bulk effective masses for CdSe ($m_e = 0.13m_o$, $m_h = 0.45m_o$)[44] and CdS ($m_e = 0.2m_o$, $m_h = 0.7m_o$)[45] were assumed. Relaxation of these assumptions is not expected to alter the main conclusions drawn from this analysis significantly. From these band offsets, the potential (V) in the shell is larger than that in the core for both the electron and the hole. This is thus a Type I heterojunction alignment, confining both carriers to the CdSe core.

The wave function analysis is restricted to the strong-confinement regime where the electron−hole Coulomb interaction is negligible in comparison to the confinement energy. The relevant Schrödinger equation is given by eq 6, where the mass, m, will depend on the carrier position in the material.

(40) Haus, J. W.; Zhou, H. S.; Honma, I.; Komiyama, H. *Phys. Rev. B* **1993**, *47*, 1359−1365.
(41) Li, J.; Wang, L.-W. *Appl. Phys. Lett.* **2004**, *84*, 3648−3650.
(42) Wei, S.-H.; Zhang, S. B.; Zunger, A. *J. Appl. Phys.* **2000**, *87*, 1304−1311.
(43) Nethercot, A. H. *Phys. Rev. Lett.* **1974**, *33*, 1088−1091.
(44) Dimmock, J. O.; Wheeler, R. G. *J. Appl. Phys.* **1961**, *32*, 2271−2277.
(45) Hopfield, J. J.; Thomas, D. G. *Phys. Rev.* **1961**, *122*, 35−52.

$$-\frac{\hbar^2}{2}\nabla\frac{1}{m}\nabla\psi(\mathbf{r}) + V(r)\psi(\mathbf{r}) = E\psi(\mathbf{r}) \quad (6)$$

The solutions to eq 6 are the linear combinations of spherical Bessel ($j_l(x)$) and Neumann ($n_l(x)$) functions for the core and shell described by eqs 7a,b. The angular dependence is given by the spherical harmonics, $Y_{ml}(\theta,\phi)$, and the particle wave vector k_n is defined as in eq 8.

$$\psi^{c}_{lm} = (A^{c}_{lm} j_l(k_c r) + B^{c}_{lm} n_l(k_c r))Y_{m\,l}(\theta,\phi) \quad (7a)$$

$$\psi^{s}_{lm} = (A^{s}_{lm} j_l(k_s r) + B^{s}_{lm} n_l(k_s r))Y_{m\,l}(\theta,\phi) \quad (7b)$$

$$k_n = \frac{\sqrt{2m_n(E - V_n)}}{\hbar} \quad (8)$$

Here, n refers to the nth layer in the material (c = core, s = shell), l and m are the angular and azimuthal quantum numbers, E is the energy of the carrier, V_n is the potential of the carrier in the nth layer (defined in absolute values relative to CdSe), and A^n_{lm} and B^n_{lm} are the coefficients determined from the boundary conditions described below. In this analysis, only the S-like "ground-state" wave functions are considered, so $l = m = 0$.

The solutions to eq 7 must satisfy the following boundary conditions: the wave function must be finite everywhere; the wave function must be continuous at the core/shell interface (eq 9a); and the probability current must be continuous at the interface between two layers separated by a finite barrier (eq 9b). These boundary conditions are sufficient to solve all of the coefficients except A^c, which is kept for normalization. The energy (E) is plotted versus eq 10 to find the roots. Normalization then completes the determination of the wave functions for the electron and the hole.

$$\psi^{c}(r_c) = \psi^{s}(r_c) \quad (9a)$$

$$\frac{1}{m_c}\frac{d}{dr}\psi^{c}(r)|_{r=r_c} = \frac{1}{m_s}\frac{d}{dr}\psi^{s}(r)|_{r=r_c} \quad (9b)$$

$$\psi^{s}(r_s) = 0 \quad (10)$$

The calculated electron and hole probability distribution functions for nanocrystals with d = 2.5 nm CdSe cores and 0.45 nm thick Co^{2+}:CdS shells are plotted in Figure 9. These results show that, at these core/shell dimensions, both carrier wave functions are attenuated in the shell region but still span the entire particle volume to some extent. The Co^{2+}−carrier overlap is thus reduced relative to an isotropic dopant distribution scenario, and this reduction translates into a reduction of the giant excitonic Zeeman splittings responsible for the MCD intensities. From these calculated wave functions, the anticipated excitonic Zeeman splitting energy for these core/shell nanocrystals can be estimated using eq 11, where c_e and c_h are the

$$\Delta E_{Zeeman} = x_{eff}\langle S_z\rangle N_0(c_e\alpha - c_h\beta) \quad (11)$$

projections of the carrier probability densities onto the dopant probability distribution function, assumed to be isotropic throughout the CdS shell layer. From Figure 9, the ratio of electron−Co^{2+} to hole−Co^{2+} projection magnitudes is 14.8:10.5. Using these calculated values of c_e = 0.148 and c_h = 0.105, and 0.179 eV and −2.71 eV for $N_0\alpha$ and $N_0\beta$, respectively,[46,47] a value of $\Delta E^{sat.}_{Zeeman} = -3.1$ meV is estimated from eq 11 for the CdSe/Co^{2+}:CdS core/shell nanocrystals. Combining the three sets of band offsets described above yields a more general estimate of $\Delta E^{sat.}_{Zeeman} = -3.0 \pm 0.2$ meV. This calculated value agrees reasonably well with the experimental result of -0.5 ± 0.2 meV, having the correct sign and being substantially smaller than those observed for the Co^{2+}:CdSe nanocrystals prepared by Synthesis III ($\Delta E^{sat.}_{Zeeman} = -13.3$ meV) or for the Co^{2+}:CdS nanocrystals prepared by Synthesis II ($\Delta E^{sat.}_{Zeeman} = -13.4$ meV).[48]

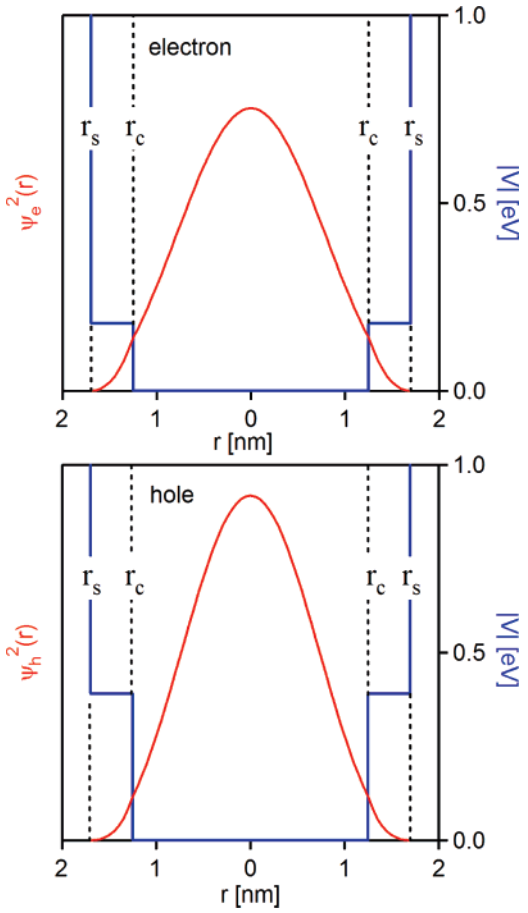

Figure 9. Conduction-band electron (top) and valence-band hole (bottom) probability distribution functions in a CdSe/CdS core/shell nanocrystal calculated as described in the text. r_c = 1.25 nm and r_s = 1.7 nm are the core and core/shell radii, respectively. The shell offsets for the conduction band (+0.18 eV) and the valence band (−0.39 eV) are plotted as their absolute values. See text for details.

The quantitative discrepancy between calculated (-3.0 ± 0.2 meV) and experimental (-0.5 ± 0.2 meV) $\Delta E^{sat.}_{Zeeman}$ for the core/shell nanocrystals of Synthesis I may arise from several possible sources, including anisotropic shell growth,[36] a dopant gradient within the shell layers, or possibly poor epitaxy at the hetero-interfaces. To this end, we note that the ligand-field transition energy and band shape reflect a uniform tetrasulfide

(46) Kacman, P. *Semicond. Sci. Technol.* **2001**, *16*, R25−R39.
(47) $N_0\beta$ in Co^{2+}:CdS could not be found in the literature. This value was therefore estimated as $N_0\beta(Co^{2+}:CdS) = [N_0\beta(Mn^{2+}:CdS)/N_0\beta(Mn^{2+}:CdSe)] \times N_0\beta(Co^{2+}:CdSe)$.
(48) As shown in ref 6, much of this reduction can be attributed to dopant displacement away from the nanocrystal core alone. For example, using the same dopant spatial distribution but setting the core/shell band offsets to zero, c_e = 0.156 and c_h = 0.157 are calculated, yielding $\Delta E^{sat.}_{Zeeman} = -4.6$ meV.

Co^{2+} coordination environment, and not a mixed sulfide/selenide coordination environment as might have been anticipated from interfaces in an isotropic distribution of dopants within a thin CdS shell like that assumed for Figure 9. Such a mixed-anion environment would be detectable as an energy shift of the Co^{2+} $^4T_1(P)$ level.[26] A dopant gradient placing all Co^{2+} ions in tetrasulfide coordination environments (i.e., removed from the CdSe/CdS interface) would further reduce the dopant−exciton overlap and could readily account for the relatively small difference between predicted and experimental $\Delta E^{sat.}_{Zeeman}$ magnitudes.

3. Excitonic Luminescence. One of the most prominent differences in physical properties between the CdSe/Co^{2+}:CdS core/shell nanocrystals (Synthesis I) and the Co^{2+}:CdS (Synthesis II) or Co^{2+}:CdSe (Synthesis III) nanocrystals is the retention of strong excitonic luminescence in the core/shell nanocrystals despite the presence of Co^{2+} luminescence traps (Figure 6). The analysis applied above to understand the weak excitonic MCD intensities in the nanocrystals prepared by Synthesis I also explains this physical difference. In the Co^{2+}:CdS and Co^{2+}:CdSe nanocrystals, the strong Co^{2+}−exciton electronic coupling responsible for the intense excitonic MCD signals also leads to rapid nonradiative excitonic relaxation to the manifold of sub-band-gap Co^{2+} ligand-field excited states, i.e., a large $k_{nr}^{Co^{2+}}$ in Scheme 1. In the CdSe/Co^{2+}:CdS core/shell nanocrystals, weak Co^{2+}−exciton electronic coupling gives rise to only weak excitonic MCD intensities but also allows k_r^{ex} to become competitive in magnitude with $k_{nr}^{Co^{2+}}$, such that ϕ_{Lum}^{ex} in eq 1 differs significantly from zero. Dopant localization at the periphery of the excitonic wave function can thus be used to modify dopant−exciton coupling magnitudes such that inverted excitonic Zeeman splittings and excitonic luminescence coexist, even for efficient luminescence traps such as Co^{2+}. This observation suggests intriguing possibilities for engineering the physical properties of quantum dots through judicious spatial localization of dopants in core/shell or related heterostructures.

IV. Discussion and Conclusion

The results presented above reveal some of the complexities that can be encountered in the synthesis and processing of doped CdSe nanocrystals. The most surprising observation is that unintended side reactions involving supposed bystander ligands in a literature procedure (SPh^- in Synthesis I) completely dictate the compositions and physical properties of the nanocrystalline products. Specifically, spectroscopic and analytical data lead to the conclusion that SPh^- decomposition during CdSe synthesis from $(Me_4N)_4[Cd_{10}Se_4(SPh)_{16}]$ and related cluster precursors generates core/shell CdSe/CdS nanocrystals, and *all* of the TM^{2+} impurity segregates into the CdS shell. Through iterative synthesis and careful spectroscopic analysis, experimental conditions that successfully yield doped CdSe nanocrystals have been identified (Synthesis III), as have conditions that successfully yield doped CdS nanocrystals via the thiolate decomposition side reaction (Synthesis II). The essential features of these syntheses are summarized in Scheme 2.

Several fascinating fundamental questions are posed by these results. Foremost among these is the question of why the TM^{2+} dopants segregate exclusively into the CdS shells. One hypothesis would be that the preexisting cobalt−SPh bonds in the $(Me_4N)_2[Co_4(SPh)_{10}]$ cluster precursor predispose this system

Scheme 2

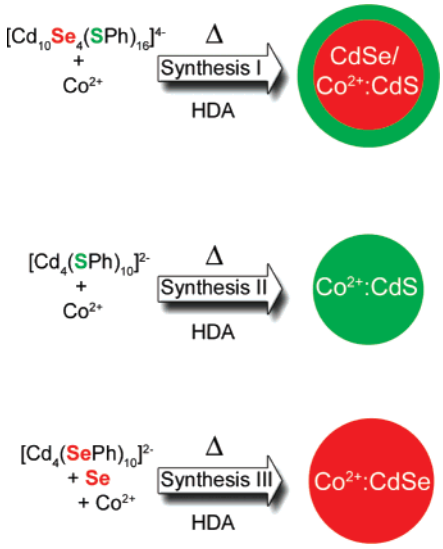

for such segregation. Control experiments show that essentially identical results are obtained from Synthesis I when $CoCl_2$ is used in place of $(Me_4N)_2[Co_4(SPh)_{10}]$, however. This result argues strongly against an important role played by the preformed Co−SPh bonds. Another hypothesis relates to the proposal that Mn^{2+} may bind preferentially to zinc blende rather than wurtzite nanocrystal surfaces.[15] It is conceivable that some or all of the CdS shell material, if grown incoherently on the CdSe surfaces, possesses the zinc blende rather than wurtzite structure. In this scenario, the difference in doping between CdSe cores and CdS shells observed here could simply reflect their different lattice structures.[49] XRD is unable to rule out this scenario because of the breadths of the diffraction peaks (Figure 1b).

An alternative explanation, and that favored by the authors, involves the intrinsic differences between Co^{2+}−S^{2-} and Co^{2+}−Se^{2-} bonding interactions, as governed for example by hard−soft acid−base (HSAB) principles.[50] According to these principles, the softer Lewis acid, Cd^{2+}, will out-compete the harder ("borderline") Co^{2+} for binding at a softer Se^{2-} surface site ($Se^{2-}_{surface}$). The HSAB bias is exacerbated by the second competition reaction that must also be considered, namely the competition between the surface and the coordinating solvent for free cations. According to HSAB principles, the coordinating solvent hexadecylamine ($:NR_3$) is a hard Lewis base and will therefore out-compete the soft $Se^{2-}_{surface}$ for coordination of the harder Lewis acid (Co^{2+}), thus shifting the reaction equilibrium away from Co^{2+} binding to the surfaces of the CdSe nanocrystals. For the softer Lewis acid (Cd^{2+}), this HSAB competition will instead favor surface coordination. The relevant HSAB competition reactions are summarized in eq 12 for the case of CdSe.

When CdS is substituted for CdSe, the harder Lewis basicity of the S^{2-} shifts the Co^{2+} surface binding equilibrium (eq 12a) to the left somewhat and simultaneously shifts the Cd^{2+} surface

(49) It is interesting to note that these nanocrystals (doped CdS shells on wurtzite CdSe cores) represent a motif reciprocal to that presented as experimental evidence for the importance of lattice structure in nanocrystal doping (doped CdSe shells on zinc blende ZnSe cores) in ref 15. Direct experimental comparison of doping in these two reciprocal core/shell motifs may therefore help elucidate the role of lattice structure in nanocrystal doping.

(50) Pearson, R. G. *J. Am. Chem. Soc.* **1963**, *85*, 3533−3539.

$$Co^{2+}-Se^{2-}_{surface} + :NR_3 \xrightleftharpoons{HSAB} Se^{2-}_{surface} + Co^{2+}-NR_3 \quad (12a)$$

$$Cd^{2+}-Se^{2-}_{surface} + :NR_3 \xleftrightharpoons{HSAB} Se^{2-}_{surface} + Cd^{2+}-NR_3 \quad (12b)$$

binding equilibrium (eq 12b) to the right. Combining these effects, HSAB chemistry thus favors Co^{2+} doping of CdS over CdSe. Anecdotal evidence in support of this HSAB interpretation of the doping results may be found in the observation that $[Co_4(SePh)_{10}]^{2-}$, the selenol congener of the cluster precursor $[Co_4(SPh)_{10}]^{2-}$, is not isolable, suggesting lower stability of the $Co^{2+}-SePh$ bond than of the $Co^{2+}-SPh$ bond.

Finally, the series of related doped semiconductor nanocrystals investigated here has provided the opportunity to explore carrier−dopant exchange interactions spectroscopically in the new motif of core/shell diluted magnetic semiconductor (DMS) heterostructures. Although the synthesis of various doped colloidal heterostructures has been described previously,[1,15,51] the interesting magneto-optical manifestations of such controlled dopant localization have not been previously described or exploited. In the present study, segregation of Co^{2+} into the CdS shell layer of CdSe/CdS core/shell nanocrystals has been demonstrated to cause a large but readily understood reduction of the CdSe excitonic Zeeman splitting, as well as a reduction in the CdSe excitonic photoluminescence quenching kinetics. The results described in this study thus demonstrate that core/shell and related nanoscale heterostructures can be used to tune exciton−dopant exchange interactions, and thereby reveal new opportunities for spin engineering and spin manipulation in DMS nanostructures using chemistry.

(51) See, for example: Wang, S.; Jarrett, B. R.; Kauzlarich, S. M.; Louie, A. Y. *J. Am. Chem. Soc.* **2007**, *129*, 3848−3856. Yang, Y.; Chen, O.; Angerhofer, A.; Cao, Y. C. *J. Am. Chem. Soc.* **2006**, *128*, 12428−12429.

Acknowledgment. This research was supported by the National Science Foundation (PECASE DMR-0239325), the Research Corporation, the Dreyfus Foundation, and the Sloan Foundation. S.A.S. received additional support through an NSF IGERT fellowship (DGE-0504573). The authors acknowledge fruitful discussions with Prof. Geoffrey Strouse (Florida State University). The authors also thank Mr. Nam Nguyen and Prof. Fumio Ohuchi (University of Washington) for assistance with XPS measurements, and Dr. Chongmin Wang (Pacific Northwest National Laboratory) for assistance with TEM measurements. TEM measurements were performed at EMSL, a national user facility sponsored by the U.S. Department of Energy's Office of Biological and Environmental Research located at PNNL and operated by Battelle.

Supporting Information Available: Additional XRD, TEM, and electronic absorption data for the Co^{2+}:CdS nanocrystals described in the text. This material is available free of charge via the Internet at http://pubs.acs.org.

JA072436L